A Dynamic Equivalent Method for PMSG Based Wind Farms Under Asymmetrical Faults

Dongsheng Li, *Student Member*, *IEEE*, Zetian Zheng, and Chen Shen, *Senior Member*, *IEEE*

***Abstract*—In this paper, a dynamic equivalent method applicable to the direct-drive permanent magnet synchronous generator (PMSG) based wind farms under asymmetrical faults is proposed. Firstly, PMSGs are clustered based on their different active power characteristics under asymmetrical faults. Further, single-machine equivalent models (SMEMs) are constructed for different clusters of PMSGs. In particular, an SMEM with multi-segmented slope recovery is introduced for PMSGs with ramp recovery characteristics. Further, a collector network equivalent method for wind farms applicable to both symmetrical and asymmetrical faults is presented. Moreover, an iterative simulation method is used to gain the required clustering indicators before the fault actually occurs. Eventually, the effectiveness of the proposed dynamic equivalent method is verified on a modified IEEE 39-bus system.**

***Index Terms*—Permanent magnet synchronous generator (PMSG), asymmetrical fault, negative-sequence control, dynamic equivalent method, anticipated contingency.**

I. Introduction

DUE to the advantages of renewability and environmental friendliness, wind power has been widely developed. However, because of the randomness and fluctuation of wind power, it can have a significant impact on the stability of the power grid [1]. Therefore, it is very important to study the impact of large-scale integration of wind power on power grids. Currently, the capacity of coal power units is generally above 100 MW, and there is no lack of coal power units with a capacity of more than 1000 MW [2]. However, the capacity of a wind turbine unit is typically 1.5 MW or 2 MW [3]. Replacing the output power of a single coal power unit would require hundreds of wind turbine units. Therefore, a wind farm generally contains tens or hundreds of wind turbines [4]. If each wind turbine is modeled in detail, it will cause problems such as large memory consumption and low simulation efficiency [5]. Hence, in order to analyze wind farms more efficiently, it is urgent to propose an accurate dynamic equivalent method for wind farms.

Nowadays, most studies focus on the equivalent modeling of wind farms under symmetrical faults. However, asymmetrical faults are the most common ones in power grids [6], [7], which will cause overvoltage on the non-faulted phase [8], [9]. In order to study the response characteristics of wind farms, equivalent models of wind farms under asymmetrical faults need to be established.

There are two types of equivalent methods for wind farms: single- and multi-machine equivalent methods. The first type of methods usually utilize indicators such as wind speed [10] and pitch angle [4] to equalize the wind farm into a single wind turbine. Nevertheless, these methods ignore the differences in response characteristics among wind turbines, making it difficult to accurately model the wind farm. Multi-machine equivalent methods first cluster wind turbines into several groups, and then establish a single-machine equivalent model (SMEM) for each cluster of wind turbines.

In the existing multi-machine equivalent method, some equivalent methods utilize wind speeds [11], [12] or geographical location [13] to cluster wind turbines. However, these methods ignore the impact of fault severity and it is inaccurate to cluster wind turbines without considering the fault conditions.

In [14] and [15], wind turbines are clustered into different groups by observing the responses of crowbar systems. However, the crowbar action characteristic in asymmetrical faults also depends on the negative-sequence voltage and negative-sequence control, making these methods challenging to be applied to asymmetrical faults. There are also methods that adopt variables such as wind speeds, terminal voltages, terminal currents [16], [17], and rotational speeds [18] as clustering indicators. Then, clustering algorithms are applied to cluster the wind turbines. Nevertheless, these indicators are all positive-sequence parameters under symmetrical faults. Due to the negative-sequence control, these positive-sequence indicators are not sufficient to reflect the operation characteristic differences among wind turbines when asymmetrical faults occur.

There are also equivalent methods that consider adaptability under asymmetrical faults. In [19], wind turbines are clustered based on their terminal voltages obtained from the power flow calculation. Furthermore, an equivalent modeling method for the zero-sequence network of the wind farm is proposed to improve the effectiveness of the equivalent mod-

Manuscript received: December 26, 2023; revised: April 13, 2024; accepted: June 14, 2024. Date of CrossCheck: June 14, 2024. Date of online publication: July 23, 2024.

This work was supported by the National Natural Science Foundation of China (No. U2166601).

This article is distributed under the terms of the Creative Commons Attribution 4.0 International License (http://creativecommons.org/licenses/by/4.0/).

D. Li and C. Shen (corresponding author) are with the Department of Electrical Engineering, Tsinghua University, Beijing 100084, China (e-mail: lids19@mails.tsinghua.edu.cn; shenchen@mail.tsinghua.edu.cn).

Z. Zheng is with the Beijing Institute of Astronautical Systems Engineering, Beijing 100076, China (e-mail: zzt_thu@qq.com).

DOI: 10.35833/MPCE.2023.001024

el under asymmetrical faults. However, this method improves the effectiveness of the equivalent method under the asymmetrical fault only by estimating the zero-sequence impedance of the collector network. Without considering the impact of the negative-sequence component and negative-sequence control, the method cannot cluster wind turbines accurately. In [20], the negative-sequence control to mitigate power and DC-link voltage oscillations is considered. An equivalent method suitable for symmetrical and asymmetrical faults is established using an improved back propagation (BP) algorithm. However, only the effectiveness of the method in solving short-circuit currents is proven. The output active power and reactive power of the wind farm are not analyzed. These studies attempt to propose equivalent methods applicable to asymmetrical faults, but all have their limitations. Moreover, there is no literature that presents the theoretical correlation between active power and fault severity under asymmetrical faults, making it hard to cluster wind turbines accurately.

Considering the fault severity and the initial operation states of PMSGs, PMSGs are clustered into three groups under symmetrical fault in [21]. At the same time, the paper proposes a method to obtain the clustering indicators before the faults occur. This method solves the problem that the clustering indicators are hard to obtain when considering the severity of the fault. However, the method in [21] cannot be used for asymmetrical faults. On the basis of [21], the negative-sequence control of PMSGs is considered in this paper, and the method is extended to asymmetrical faults. Currently, there are two commonly used negative-sequence control methods, one for mitigating active power and DC-link voltage oscillations [22], [23], and the other for balancing the grid voltage by reducing the negative-sequence voltage [8], [24]. In this paper, the above two negative-sequence control methods are analyzed to find the correspondence between external fault conditions and wind turbine response characteristics based on PMSGs. The equivalent method proposed in this paper is a multi-machine equivalent method, which can be divided into two parts: clustering and equivalent modeling. The equivalent modeling method is similar in meaning to the "aggregated approach", both involving aggregating wind turbines within the same cluster into one equivalent unit. In the equivalent modeling process, the recovery characteristics of PMSGs are considered. Moreover, this paper presents an equivalent method for collector network that is applicable to both symmetrical and asymmetrical faults. Further, the clustering indicators are calculated by an iterative simulation method under asymmetrical faults, making the method applicable to anticipated contingencies. The main contributions of this paper are given as follows.

1) Using positive- and negative-sequence terminal voltages and wind speeds as clustering indicators, a clustering method is proposed for PSMGs under asymmetrical faults. All possible response characteristics under two different negative control methods are analyzed. Further, the clustering boundaries are derived theoretically.

2) This paper extends the existing modeling method to asymmetrical faults. It also proposes an improved equivalent method for collector network based on equal average voltage drop, which ensures the consistency of the output reactive power before and after equivalence.

3) An iterative simulation for solving the positive- and negative-sequence terminal voltages is presented. Under asymmetrical faults, due to the presence of negative-sequence control, it is necessary to further calculate negative-sequence indicators and compare them with existing methods. Based on the proposed dynamic equivalent method and the decoupled sequence network, the clustering indicators can be obtained before the fault actually occurs.

The paper is organized as follows. The structure and control method of the PMSG is presented in Section II. The clustering boundaries for the PMSG are introduced in Section III. The dynamic equivalent method for PMSG based wind farms is proposed in Section IV. An iterative simulation method for solving clustering indicators is introduced in Section V. The method verification is demonstrated in Section VI. Conclusions are summarized in Section VII.

II. Structure and Control Method of PMSG

This section will introduce the structure and the two commonly used negative-sequence control methods of the PMSG applied in this paper.

The structure of the PMSG adopted in this paper is the same as that in [21]. As for the control system, the machine-side converter of the PMSG can control the terminal current of the synchronous generator according to the boost circuit, thereby changing the rotor speed to ensure that the wind turbine operates at the optimal tip speed ratio state, achieving the maximum power point tracking (MPPT) control. On the DC side, when the voltage of DC capacitor reaches the threshold, the chopper circuit will operate to prevent overvoltage. The control method of the grid-side converter (GSC) will be introduced in the following parts. The topology and control method of the permanent magnet synchronous generator (PMSG) are shown in Fig. 1, where SVPWM represents the space vector pulse width modulation; and PR represents the proportional resonant controller.

A. Negative-sequence Control for Mitigating Imbalance of Grid Voltage

During normal operation, PMSG adopts the positive-sequence voltage-oriented vector control. At this time, the active power and reactive power are controlled by the d-axis current and the q-axis current, respectively. The reference value of active power is determined by the constant capacitor voltage control. In order to meet the unit power factor control, the reactive power is generally 0.

When an asymmetrical fault occurs, the PMSG needs to inject an appropriate amount of positive-sequence reactive current into the power grid and absorb negative-sequence reactive current from the power grid to reduce the imbalance degree of grid voltage according to the grid code [25]. The reference values of the positive- and negative-sequence reactive currents are:

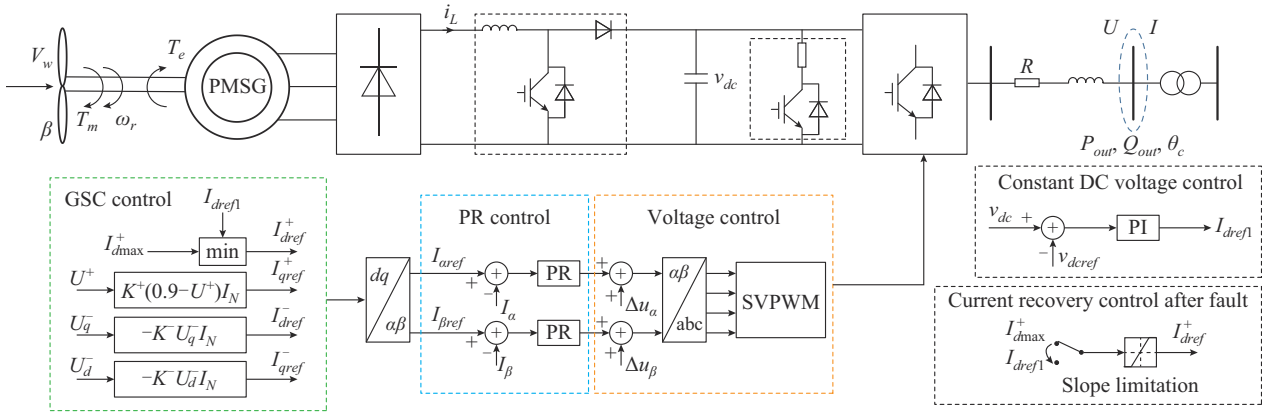

Fig. 1. Topology and control method of PMSG.

$$\begin{cases} I_t^+ = K^+\left(0.9 - U^+\right) I_N \\ I_t^- = K^- U^- I_N \end{cases} \tag{1}$$

where the superscripts "+" and "–" denote the positive- and negative-sequence components, respectively; I_t^+ is the reference value of positive-sequence reactive current injected by the PMSG; I_t^- is the reference value of negative-sequence reactive current absorbed by the PMSG; K^+ and K^- are the positive- and negative-sequence reactive current factors, respectively; U^+ and U^- are the magnitudes of positive- and negative-sequence voltages, respectively; and I_N is the rated current of the PMSG.

After meeting the requirement of the grid code, the remaining capacity of the converter should be used to output the maximum possible positive-sequence active power to maintain the stability of the DC-link capacitor voltage [24]. Meanwhile, the negative-sequence active current is maintained at 0. Thus, the reference values of negative-sequence current and positive-sequence q-axis current can be derived by:

$$\begin{cases} I_{ref}^- = I_t^- \\ I_{qref}^+ = I_t^+ \end{cases} \tag{2}$$

where I_{ref}^- and I_{qref}^+ are the reference values of negative-sequence current and positive-sequence q-axis current, respectively.

In order to keep the output current within the maximum current limit of the converter, the positive- and negative-sequence currents should satisfy the following inequality:

$$\left|I_{ref}^-\right| + \left|I_{ref}^+\right| \le I_{\max} \tag{3}$$

where I_{ref}^+ is the reference value of positive-sequence current; and $I_{\max}$ is the maximum current limit of the converter. Combining (1)-(3), the reference value of positive-sequence active current can be derived by:

$$\begin{cases} I_{dref}^+ = \min\left\{I_{dref1}, I_{d\max}^+\right\} \\ I_{d\max}^+ = \sqrt{\left(I_{\max} - K^- U^- I_N\right)^2 - \left(I_{qref}^+\right)^2} \end{cases} \tag{4}$$

where I_{dref}^+ is the reference value of the positive-sequence d-axis active current; I_{dref1} is determined by the constant DC voltage control; and $I_{d\max}^+$ is the maximum allowable positive-sequence d-axis current.

In summary, the positive- and negative-sequence dq-axis components of the current can be derived by:

$$\begin{cases} I_{dref}^+ = \min\left\{I_{dref1}, I_{d\max}^+\right\} \\ I_{qref}^+ = K^+\left(0.9 - U^+\right) I_N \quad 0.2 \le U^+ \le 0.9 \\ I_{dref}^- = -K^- U_q^- I_N \\ I_{qref}^- = -K^- U_d^- I_N \end{cases} \tag{5}$$

where I_{dref}^- and I_{qref}^- are the reference values of the negative-sequence d- and q-axis terminal current of the PMSG, respectively; and U_d^- and U_q^- are the negative-sequence d- and q-axis components of the terminal voltage in per unit, respectively.

Under the above negative-sequence control method, the PMSG can inject and absorb the required reactive power while outputting the positive-sequence active power to maintain the stability of the DC-link capacitor voltage. If the positive-sequence active current is less than the normal operation value due to the converter capacity limitation after the fault clears, the rising rate of the active current is restricted to reduce the mechanical stress on the PMSG [26], [27].

B. Negative-sequence Control for Mitigating Oscillation of Active Power

The instantaneous power can be deduced as:

$$\begin{cases} P_{out} = P_{out0} + P_{c2}\cos 2\theta_c + P_{s2}\sin 2\theta_c \\ Q_{out} = Q_{out0} + Q_{c2}\cos 2\theta_c + Q_{s2}\sin 2\theta_c \end{cases} \tag{6}$$

where θ_c is the grid angle, which can be presented as $\theta_c = \omega t$, and ω is the grid angular frequency; P_{out0} is the average active power in P_{out}; Q_{out0} is the average reactive power in Q_{out}; and P_{c2}, P_{s2}, Q_{c2}, and Q_{s2} are the coefficients of the second-harmonic components of the active and reactive power, respectively. Some of them can be derived as:

$$\begin{bmatrix} P_{out0} \\ Q_{out0} \\ P_{c2} \\ P_{s2} \end{bmatrix} = \frac{3}{2}\begin{bmatrix} U_d^+ & U_q^+ & U_d^- & U_q^- \\ U_q^+ & -U_d^+ & U_q^- & -U_d^- \\ U_d^- & U_q^- & U_d^+ & U_q^+ \\ U_q^- & -U_d^- & -U_q^+ & U_d^+ \end{bmatrix}\begin{bmatrix} I_d^+ \\ I_q^+ \\ I_d^- \\ I_q^- \end{bmatrix} \tag{7}$$

where U_d^+, U_q^+, U_d^-, and U_q^- are the positive- and negative-sequence dq-axis terminal voltages, respectively.

When using negative-sequence control for mitigating second-harmonic components of the active and reactive power, the reference values of currents can be derived by:

$$\begin{bmatrix} I_{dref}^{+} \\ I_{qref}^{+} \\ I_{dref}^{-} \\ I_{qref}^{-} \end{bmatrix} = \begin{bmatrix} U_d^{+} & U_q^{+} & U_d^{-} & U_q^{-} \\ U_q^{+} & -U_d^{+} & U_q^{-} & -U_d^{-} \\ U_d^{-} & U_q^{-} & U_d^{+} & U_q^{+} \\ U_q^{-} & -U_d^{-} & -U_q^{+} & U_d^{+} \end{bmatrix}^{-1} \times \frac{2}{3} \begin{bmatrix} P_{ref} \\ Q_{ref} \\ 0 \\ 0 \end{bmatrix} \tag{8}$$

where P_{ref} and Q_{ref} are the reference values of average active and reactive power of the PMSG, respectively.

For convenience of calculation, the reference value of reactive power is set to be 0. Additionally, in order to maintain the DC-link voltage, the reference value of the active power is set as the normal operation value. If the output active power is limited by the converter capacity, the reference value of active power will be set as the maximum value within the converter capacity. At this time, the reference values of currents can be derived by:

$$\begin{bmatrix} I_{dref}^{+} \\ I_{qref}^{+} \\ I_{dref}^{-} \\ I_{qref}^{-} \end{bmatrix} = \frac{2P_{ref}}{3D} \begin{bmatrix} U_d^{+} \\ U_q^{+} \\ -U_d^{-} \\ -U_q^{-} \end{bmatrix} \tag{9}$$

where P_{ref} and D can be expressed as:

$$P_{ref} = \min\left\{P_0, P_{\max}\right\} \tag{10}$$

$$D = \left(U_d^{+}\right)^2 + \left(U_q^{+}\right)^2 - \left(U_d^{-}\right)^2 - \left(U_q^{-}\right)^2 \tag{11}$$

where P_0 is the active power before the fault occurs; and $P_{\max}$ is the maximum active power under converter capacity limitation, which will be introduced in Section III.

III. Clustering Boundaries for PMSG

In this section, the active power dynamic response characteristics of a single PMSG will be classified in various operation scenarios, considering the negative-sequence control. Under different control methods, the meanings of *dq*-axis reference currents remain the same, but the expressions differ.

A. Clustering Boundaries Under Negative-sequence Control for Mitigating Imbalance of Grid Voltage

If the converter capacity is sufficient, the active power of the PMSG will restore to the normal operation power during the fault. If the external fault is severe, most of the converter capacity is used to mitigate the imbalance of grid voltage. The output active power of the PMSG is limited by the converter capacity and unable to reach the normal operation value. Therefore, during the fault period, we can divide the active power of PMSGs into two clusters. The active power can restore to the normal operation power or the active power is restricted by the converter capacity.

Since the energy accumulated by the second-harmonic component of active power on the DC-link capacitor in one cycle is almost 0, it can be considered that the DC-link capacitor voltage is only related to the average active power. To identify the operation boundaries of these two response characteristics, we have hypothesized a critical operation condition. When the average output active power during the fault is equal to the normal operation value, and the current of the converter is equal to the maximum value at the same time, the normal operation power is the critical active power of these two clusters of response characteristics under the fault. It can be considered that the actual currents are the same as the reference values owing to the fast control of the PMSG [28]. Therefore, the initial critical active power is given as:

$$\begin{cases} P_0 = P_{fault} = P_{cri1} \\ I_{dref}^{+} = I_{d\max}^{+} \\ P_{fault} = \dfrac{3}{2}\left(I_{dref}^{+}U_d^{+} + I_{qref}^{+}U_q^{+} + I_{dref}^{-}U_d^{-} + I_{qref}^{-}U_q^{-}\right) \end{cases} \tag{12}$$

where P_{fault} is the average active power of the PMSG during the fault; and P_{cri1} is the first critical active power. Due to the positive-sequence voltage-oriented vector control, U_q^{+} is equal to 0. Substituting (4) and (5) into (12), P_{cri1} can be derived as:

$$\begin{cases} I_{d\max}^{+} = \sqrt{\left(I_{\max} - K^{-}U^{-}I_N\right)^2 - \left[K^{+}\left(0.9 - U^{+}\right)I_N\right]^2} \\ P_{cri1} = \dfrac{3}{2} I_{d\max}^{+} U^{+} \end{cases} \tag{13}$$

After the fault clears, the positive-sequence voltage amplitude is close to 1. When $P_0 > P_{cri1}$, the active power is less than the normal operation value during the fault. At this time, we can obtain $I_{dref}^{+} = I_{d\max}^{+}$ according to (4). If the positive-sequence *d*-axis current at the moment of fault clearance I_{dref}^{+} is higher than the *d*-axis current during the normal operation I_{d0}, the active power will exceed P_0 and restore to P_0 due to voltage restoration after the fault clears. If $I_{dref}^{+} < I_{d0}$, the active power will recover at a fixed rate.

The second critical initial active power is to determine whether the PMSG will recover at a fixed rate, which can be derived by:

$$\begin{cases} I_{d\max}^{+} = I_{d0} = I_{dcri2} \\ P_{cri2} = \dfrac{3}{2} I_{dcri2} U_{d0}^{+} \end{cases} \tag{14}$$

where I_{dcri2} is the second initial critical *d*-axis current; P_{cri2} is the second critical active power; and U_{d0}^{+} is the positive-sequence voltage before the fault starts, which is approximate to 1.

Based on the above analysis, the characteristics of active power are divided into the following three clusters.

1) When $P_0 < P_{cri1}$, $I_{dref}^{+} = I_{dref1}$. The average active power is the same as P_0 during the fault, which can maintain the capacitor voltage stability.

2) When $P_{cri1} \le P_0 < P_{cri2}$, $I_{dref}^{+} = I_{d\max}^{+}$. The average active power is less than P_0 during the fault.

3) When $P_0 \ge P_{cri2}$, $I_{dref}^{+} = I_{d\max}^{+}$. The average active power will recover at a limited slope after the fault.

The characteristics of active power of PMSG are shown schematically in Fig. 2. The blue curve represents the active power response characteristics, while the red curve shows the average active power. t_0 is the time of fault start; t_c is the time of fault clearance; and t_n is the time when the PMSG restores to normal operation.

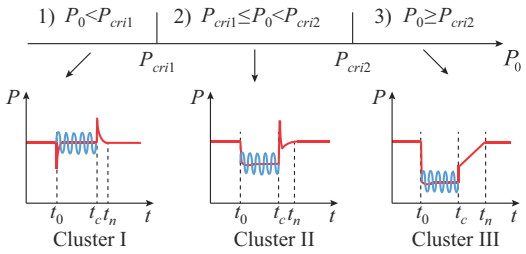

Fig. 2. Characteristics of active power of PMSG.

Further, we can obtain the critical wind speeds V_{cri1} and V_{cri2} according to the wind power curve:

$$\begin{cases} V_{cri1}=f^{-1}\left(P_{cri1}\right) \\ V_{cri2}=f^{-1}\left(P_{cri2}\right) \end{cases} \tag{15}$$

where f^{-1} is the inverse function of the wind power curve.

According to (13) and (14), the clustering boundaries are shown in Fig. 3. The two orange planes above and below refer to the rated wind speed V_n and the cut-in wind speed V_c of the PMSG, respectively. The orange plane perpendicular to the U^+-U^- plane represents the situation where the positive- and negative-sequence voltage drops are equal. The positive-sequence voltage is usually greater than the negative-sequence voltage during an asymmetrical fault, so only the right-hand part of the plane needs to be analyzed. The three clusters I-III labeled in Fig. 3 correspond to the three clusters in Fig. 2.

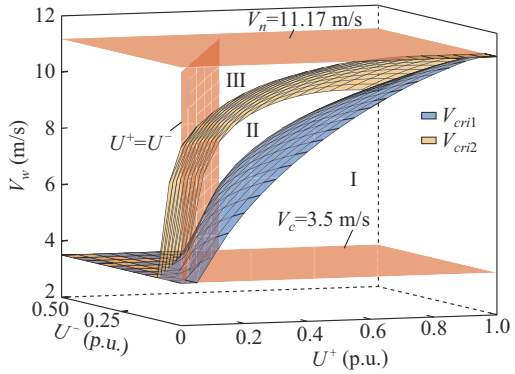

Fig. 3. Clustering boundaries under control for mitigating imbalance of grid voltage.

In order to show the clustering boundaries more clearly, we take the case where the negative-sequence voltage drops to 0.2 p.u. as an example, and draw the clustering boundaries based on the positive-sequence voltage and the wind speed, as shown in Fig. 4. When the positive- and negative-sequence terminal voltages and the operation wind speed of a PMSG are known, it can be quickly determined which cluster the PMSG belongs to.

B. Clustering Boundaries Under Negative-sequence Control for Mitigating Oscillations of Active Power

Under the negative-sequence control for mitigating the second-harmonic component of active power, the response characteristics of the PMSG can also be divided into three clusters, as shown in Fig. 2.

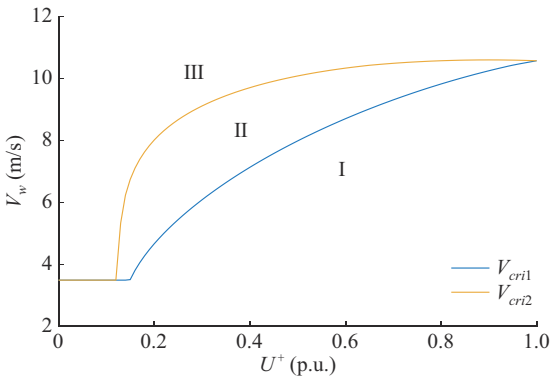

Fig. 4. Clustering boundaries when $U^-=0.2$ p.u..

By comparing the maximum output active power during the fault with the active power during normal operation, it can be determined whether the active power characteristics belong to Cluster I or Cluster II. When the PMSG outputs the maximum active power, the positive- and negative-sequence currents should satisfy:

$$\sqrt{\left(I_{dref}^{+}\right)^2+\left(I_{qref}^{+}\right)^2}+\sqrt{\left(I_{dref}^{-}\right)^2+\left(I_{qref}^{-}\right)^2}=I_{\max} \tag{16}$$

Substituting (9) into (16), we can obtain:

$$\frac{2P_{\max}}{3D}\left(U^{+}+U^{-}\right)=I_{\max} \tag{17}$$

By simplifying (17), P_{cri1} can be derived by:

$$\begin{cases} P_{cri1}=P_{\max} \\ P_{\max}=\dfrac{3}{2}\left(U^{+}-U^{-}\right)I_{\max} \end{cases} \tag{18}$$

Similarly, comparing the magnitude of the positive-sequence d-axis current at the moment of fault clearance with I_{d0}, we can determine whether the active power will restore at the specified slope. In order to solve the second critical current, the reference active power is equal to the maximum active power during the fault ($P_{ref}=P_{\max}$) at this time. The second critical initial active power can be derived by:

$$\begin{cases} I_{dcri2}=I_{dref}^{+} \\ I_{dref}^{+}=2P_{\max}U_d^{+}/(3D) \end{cases} \tag{19}$$

Substituting $P_{\max}$ into (19), we can obtain:

$$\begin{cases} I_{dcri2}=U_d^{+}I_{\max}/\left(U^{+}+U^{-}\right) \\ P_{cri2}=\dfrac{3}{2}I_{dcri2}U_{d0}^{+} \end{cases} \tag{20}$$

The clustering boundaries considering the negative-sequence control mentioned above are shown in Fig. 5.

IV. Dynamic Equivalent Method for PMSG Based Wind Farms

This section will introduce the dynamic equivalent method for the three clusters of PMSGs above. Moreover, a collector network equivalent method suitable for practical wind farms is proposed in Section IV-C.

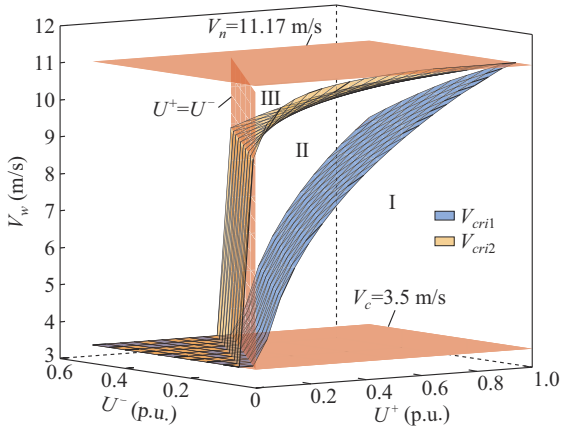

Fig. 5. Clustering boundaries under control for mitigating oscillations of active power.

A. Capacity Weighted Equivalent Modeling

The capacity weighted equivalent modeling is always employed to aggregate the wind turbines in the same cluster [16], [29]. For the PMSGs in Clusters I and II shown in Fig. 2, the accumulated active power of PMSGs is consistent with that of a single PMSG.

Thus, the two clusters of PMSGs can be equalized by capacity weighted equivalent modeling. The effectiveness of this method has been theoretically analyzed in [30]. The equivalent parameters can also be found in [30].

B. Dynamic Equivalent Method Considering Slope Recovery of PMSGs Under Asymmetrical Faults

In this subsection, a dynamic equivalent method is applied for PMSGs in Cluster III to more accurately reflect the characteristics of the wind farm during fault recovery periods. Due to the differences in terminal voltage and wind speed for each PMSG in Cluster III, the duration of the slope recovery process also varies. Similar to the idea in [21], the slope duration of each PMSG needs to be calculated to control the equivalent machine accordingly. Taking the negative-sequence control for mitigating the imbalance of grid voltage as an example, the slope duration can be derived by:

$$T_i = \frac{1}{k}\left(I_{d0i} - I_{dcri2,i}\right) \tag{21}$$

where T_i is the slope recovery duration of the i^{th} PMSG; $I_{dcri2,i}$ is the second initial critical d-axis current of the i^{th} PMSG; I_{d0i} is the d-axis current during the normal operation of the i^{th} PMSG; and k is the limited maximum rising rate of the d-axis current.

The initial currents of PMSGs can be derived by:

$$\begin{cases} P_{0i} = f\left(V_{wi}\right) \\ I_{d0i} = \dfrac{2P_{0i}}{3U_{d0}^{+}} \end{cases} \tag{22}$$

where P_{0i} is the active power of the i^{th} PMSG before the fault occurs; and V_{wi} is the wind speed of the i^{th} PMSG.

Under an asymmetrical fault, the positive-sequence d-axis current at the end of the fault is determined by both the positive- and negative-sequence voltages, which can be calculated by:

$$\begin{cases} t_i = \dfrac{1}{k}\left(\dfrac{2f\left(V_{\text{wi}}\right)}{3e} - I_{dcri2,i}\right) \\ I_{dcri2,i} = \sqrt{\left(I_{\max} - K^{-}U_i^{-}I_N\right)^2 - \left[K^{+}\left(0.9 - U_i^{+}\right)I_N\right]^2} \end{cases} \tag{23}$$

where e is the magnitude of grid voltage space vector during normal operation. After ranking all PMSG slope recovery durations, the rising rate of the equivalent d-axis current can be limited by:

$$k_{lim} = \left(N_3 - n + 1\right)k \quad t_{n-1} \le t < t_n \tag{24}$$

where N_3 is the total number of PMSGs in Cluster III; and t is the time from the moment of fault clearance. The recovery rate is maintained at k when $t \ge t_{N_3}$ to model the overshoot process of the constant DC-link voltage control. The schematic diagram of the proposed dynamic equivalent method is shown in Fig. 6.

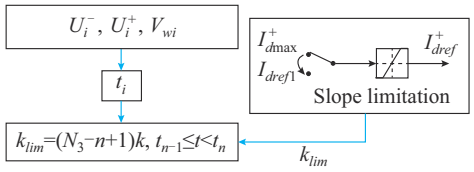

Fig. 6. Schematic diagram of proposed dynamic equivalent method.

C. Collector Network Equivalent Method

This subsection improves the traditional collector network equivalent method based on equal average voltage drop [31]. The collector network equivalent method ensures that the output reactive power of the wind farm remains consistent before and after equivalence.

The traditional collector network equivalent method based on equal average voltage drop calculates the average voltage drop weighted by the output active power of PMSGs. The collector network parameters can be derived by:

$$\begin{cases} \dot{U}_{ave} = \dfrac{\sum_{i=1}^{N} P_i \dot{U}_i}{\sum_{i=1}^{N} P_i} \\ Z_{eq} = \dfrac{\dot{U}_{pcc} - \dot{U}_{ave}}{\sum_{i=1}^{N} \dot{I}_i} \end{cases} \tag{25}$$

where $\dot{U}_{ave}$ is the average voltage drop of PMSGs; $\dot{U}_i$ is the terminal voltage phasor of the i^{th} PMSG; N is the total number of PMSGs; P_i is the output active power of the i^{th} PMSG; Z_{eq} is the parameter of the equivalent collector network; $\dot{U}_{pcc}$ is the voltage at the point of common coupling (PCC); and $\dot{I}_i$ is the output current of the i^{th} PMSG.

However, as the output active power of each PMSG continuously changes, the equivalent network parameters also vary during a fault, making them challenging to be implemented effectively. Moreover, under asymmetrical fault, the terminal voltage contains second-harmonic components, making it difficult to directly calculate the equivalent network parameters through the terminal voltage. Therefore, we pro-

pose an improved method by ensuring consistency in the output reactive power before and after the equivalence.

In the positive-sequence network, the sum of the output reactive current of each PMSG can be derived by:

$$I_q = \sum_{i=1}^{N} k\left(0.9 - \left|\dot{U}_i^+\right|\right) I_{N,i} \tag{26}$$

where $I_{N,i}$ is the rated current of the i^{th} PMSG; $\dot{U}_i^+$ is the positive-sequence terminal voltage phasor of the i^{th} PMSG.

Since the rated current of the equivalent PMSG is the sum of the rated currents of each PMSG, the output reactive current of the equivalent PMSG during a fault can be derived by:

$$I_{q,eq} = k\left(0.9 - \left|\dot{U}_{eq}^+\right|\right) \sum_{i=1}^{N} I_{N,i} \tag{27}$$

where $\dot{U}_{eq}^+$ is the terminal voltage of the equivalent PMSG in the positive-sequence network.

To ensure that the output reactive current of the wind farm is equal before and after equivalence, $\dot{U}_{eq}^+$ can be solved through (26) and (27):

$$\left|\dot{U}_{eq}^+\right| = \frac{\sum_{i=1}^{N} I_{N,i}\left|\dot{U}_i^+\right|}{\sum_{i=1}^{N} I_{N,i}} = \frac{\sum_{i=1}^{N} S_i\left|\dot{U}_i^+\right|}{\sum_{i=1}^{N} S_i} \tag{28}$$

where S_i is the capacity of the i^{th} PMSG. Therefore, we can calculate the average voltage drop weighted by the rated capacity of each PMSG. It will not only make the calculation more convenient but also ensures the consistency of the output reactive power before and after equivalence during a fault. Based on this, the equivalent collector network parameters can be derived by:

$$\begin{cases} \dot{U}_{eq}^+ = \dfrac{\sum_{i=1}^{N} S_i \dot{U}_i^+}{\sum_{i=1}^{N} S_i} \\ Z_{eq} = \dfrac{\dot{U}_{pcc}^+ - \dot{U}_{eq}^+}{\sum_{i=1}^{N} \dot{I}_i^+} \end{cases} \tag{29}$$

where $\dot{U}_{pcc}^+$ is the positive-sequence PCC voltage; and $\dot{I}_i^+$ is the positive-sequence output current of the i^{th} PMSG.

Since the positive- and negative-sequence parameters of the wind farm collector network are the same, we use the results calculated under the positive-sequence network as the parameters of the equivalent network. The collector network equivalent method in this subsection requires parameters such as the terminal voltage and the output current of each PMSG, which will be introduced in Section V.

V. Solution to Clustering Indicators

In this paper, the clustering indicators are the positive-sequence terminal voltages, negative-sequence terminal voltages, and wind speeds. The wind speeds can be acquired by prediction or measurement. However, the positive- and negative-sequence terminal voltages are generally difficult to obtain before the fault actually occurs. In this section, the solution to positive- and negative-sequence terminal voltages is presented, assuming that the PCC voltage is known. Then, the actual PCC voltage is calculated by iterative simulation. Eventually, the equivalent model of the wind farm can be obtained.

A. Calculation of Terminal Voltages

The calculation method is introduced in a real wind farm topology, as shown in Fig. 7.

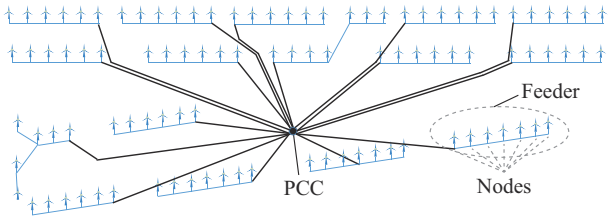

Fig. 7. Wind farm topology.

Due to the fast response of PMSGs, the terminal voltages can be calculated by the static model of PMSGs when the PCC voltage is known. In this subsection, we take the negative-sequence control for mitigating the imbalance of grid voltages as an example.

We decouple the positive- and negative-sequence networks to calculate the positive- and negative-sequence terminal voltages, respectively. According to (5), the output *d*- and *q*-axis currents of the PMSG in the negative-sequence network are only related to the negative-sequence voltage dips, while the *d*-axis current in the positive-sequence network is affected by both positive- and negative-sequence voltages. Therefore, we can calculate the negative-sequence terminal voltage under the negative-sequence network first, and then calculate the positive-sequence terminal voltage.

1) Solution to Negative-sequence Terminal Voltages

In the negative-sequence network, the power of PMSGs can be derived by:

$$\begin{cases} P_i^- = 1.5\left(U_{di}^- I_{drefi}^- + U_{qi}^- I_{qrefi}^-\right) \\ Q_i^- = 1.5\left(U_{qi}^- I_{drefi}^- - U_{di}^- I_{qrefi}^-\right) \end{cases} \tag{30}$$

where P_i^- and Q_i^- are the output active and reactive power in the negative-sequence network, respectively; U_{di}^- and U_{qi}^- are the negative-sequence *d*- and *q*-axis terminal voltages of the i^{th} PMSG, respectively; and I_{drefi}^- and I_{qrefi}^- are the reference values of the negative-sequence *d*- and *q*-axis terminal currents of the PMSG, respectively. Substituting (5) into (30), we can obtain:

$$\begin{cases} P_i^- = 0 \\ Q_i^- = -1.5K^-\left(\left(U_{qi}^-\right)^2 + \left(U_{di}^-\right)^2\right) I_N = -1.5K^-\left(U_i^-\right)^2 I_N \end{cases} \tag{31}$$

where U_i^- is the negative-sequence terminal voltage phasor of the i^{th} PMSG. The output current of PMSG can be derived by:

$$\dot{I}_{ni}^{-}=\left(\frac{P_i^{-}+\mathrm{j}Q_i^{-}}{\dot{U}_i^{-}}\right)^{*} \tag{32}$$

where $\dot{I}_{ni}^{-}$ and $\dot{U}_i^{-}$ are the output current and the negative-sequence terminal voltage of the i^{th} PMSG in the negative-sequence network, respectively.

Further, when the PCC voltage is known, it can be regarded as the voltage reference node. The updated terminal voltages of PMSGs are:

$$\dot{U}'^{-}=\dot{U}_{pcc}^{-}+Z\dot{I}_n^{-} \tag{33}$$

where $\dot{U}_{pcc}^{-}$ is the PCC voltage in the negative-sequence network; $\dot{U}'^{-}$ is the updated negative-sequence terminal voltage; and $\dot{I}_n^{-}$ is the injected current composed of $\dot{I}_{ni}^{-}$.

Since the injected currents of PMSGs are related to their terminal voltages, the negative-sequence terminal voltages can be solved by iterative method. The specific steps are as follows.

Step 1: initialize the negative-sequence terminal voltages of PMSGs and let $\dot{U}_i^{-}=\dot{U}_{pcc}^{-}$.

Step 2: update the negative-sequence terminal voltages according to (31)-(33).

Step 3: if $\left|\dot{U}'^{-}-\dot{U}^{-}\right|<\sigma_1$, where σ_1 is the allowable error of negative-sequence terminal voltages, the negative-sequence terminal voltages of all PMSGs are available in $\dot{U}'^{-}$. Otherwise, let $\dot{U}^{-}=\dot{U}'^{-}$ and go to *Step 2*.

2) Solution to Positive-sequence Terminal Voltages

In the positive-sequence network, the output power of PMSGs can be derived by:

$$\begin{cases}P_i^{+}=1.5\left(U_{di}^{+}I_{drefi}^{+}+U_{qi}^{+}I_{qrefi}^{+}\right)\\ Q_i^{+}=1.5\left(U_{qi}^{+}I_{drefi}^{+}-U_{di}^{+}I_{qrefi}^{+}\right)\end{cases} \tag{34}$$

where U_{di}^{+} and U_{qi}^{+} are the positive-sequence d- and q-axis terminal voltages of the i^{th} PMSG, respectively; and I_{drefi}^{+} and I_{qrefi}^{+} are the reference values of the positive-sequence d- and q-axis terminal currents of the PMSG, respectively. The reference values of the current are rewritten as:

$$\begin{cases}I_{qrefi}^{+}=K^{+}\left(0.9-U_i^{+}\right)I_N\\ I_{drefi}^{+}=\min\left\{I_{dref1i},I_{d\max i}\right\}\\ I_{d\max i}=\sqrt{\left(I_{\max}-K^{-}\left|U_i^{-}\right|I_N\right)^2-\left(I_{qrefi}^{+}\right)^2}\end{cases} \tag{35}$$

where I_{dref1i} is the d-axis current reference value of the constant DC-link capacitor voltage control; and $I_{d\max i}$ is the maximum allowable positive-sequence d-axis current of the i^{th} PMSG. In order to maintain the DC voltage, the following equation should be satisfied:

$$U_{d0}^{+}I_{d0i}=U_i^{+}I_{dref1i} \tag{36}$$

While U_{d0}^{+} is close to 1, I_{dref1i} can be derived by:

$$I_{dref1i}=\frac{I_{d0i}}{U_i^{+}} \tag{37}$$

Since U_i^{-} has been solved in the previous subsection, the positive-sequence output currents of PMSGs are only related to the positive-sequence terminal voltages. According to (35)-(37), we can also solve the positive-sequence terminal voltages in the same way. As a result, if the PCC voltage is known, we can obtain the positive- and negative-sequence terminal voltages of PMSGs by the solution method mentioned above.

B. Iterative Simulation for Solving PCC Voltage

An iterative simulation for solving the PCC voltage is presented in this subsection. The simulation can obtain the PCC voltage before the fault occurrence, which avoids the simulation of the detailed method (DM) to obtain the clustering indicators. The specific steps are shown as follows.

Step 1: set $U_{pcc}^{+}=1$ and $U_{pcc}^{-}=0$.

Step 2: let $\dot{U}_{pcc}^{+}=U_{pcc}^{+}\angle 0°$ and $\dot{U}_{pcc}^{-}=U_{pcc}^{-}\angle 0°$. Use the method introduced above to calculate the positive- and negative-sequence terminal voltages of PMSGs.

Step 3: establish the equivalent model of the wind farm according to Section IV.

Step 4: the anticipated contingency is simulated based on the equivalent model. Furthermore, the positive- and negative-sequence PCC voltages at the moment of the fault clearance ($U_{pcc}^{+\prime}$ and $U_{pcc}^{-\prime}$) can be obtained by the simulation result.

Step 5: if $\left|U_{pcc}^{+\prime}-U_{pcc}^{+}\right|<\sigma_2$ and $\left|U_{pcc}^{-\prime}-U_{pcc}^{-}\right|<\sigma_2$, where σ_2 is the allowable error, go to *Step 6*; otherwise, set $U_{pcc}^{+}=U_{pcc}^{+\prime}$, $U_{pcc}^{-}=U_{pcc}^{-\prime}$, and go to *Step 2*.

Step 6: once the actual PCC voltage is solved, clustering indicators of each PMSG can be obtained, and the equivalent model of the wind farm can be established.

In summary, the overall process of the proposed dynamic equivalent method is illustrated in Fig. 8.

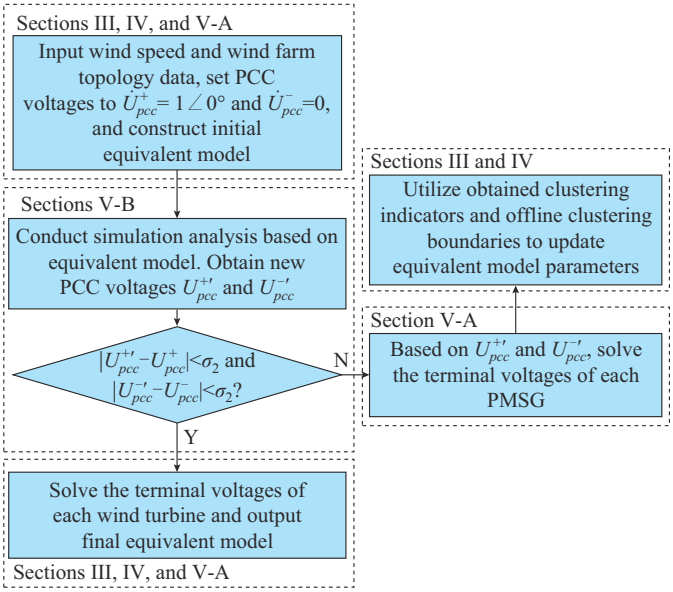

Fig. 8. Overall process of proposed dynamic equivalent method.

VI. Method Verification

The proposed dynamic equivalent method is analyzed on the CloudPSS platform [32], [33] in a modified IEEE 39-bus system, as shown in Fig. 9. A wind farm including 100 PMSGs is studied, as shown in Fig. 7.

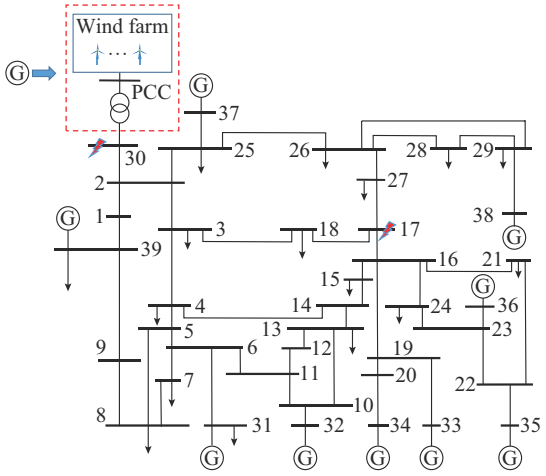

Fig. 9. A modified IEEE 39-bus system.

A. Case I: Two-phase Short-circuit Fault at Bus 30

A two-phase short-circuit fault occurs between phases B and C at bus 30, lasting for 0.2 s. The ground resistance is 0.001 Ω. The wind speeds of PMSGs are shown in Fig. 10, which are modeled with the Jensen model.

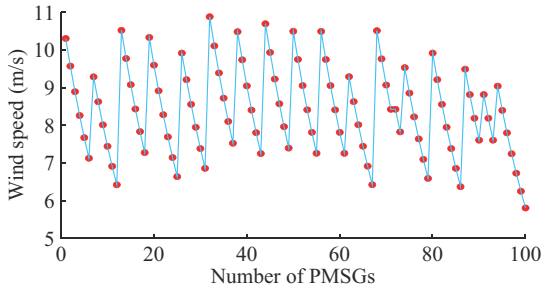

Fig. 10. Wind speeds of PMSGs in Case I.

The PCC voltage is calculated by iterative simulation and the iteration result is shown in Table I. The PCC voltage converges after two iterations of simulation with the equivalent model. Then, we can further compute the terminal voltages of PMSGs, as shown in Fig. 11. The maximum percentage error is 0.089%. After obtaining the terminal voltages of each wind turbine, the collector network parameters can be calculated by the method described in Section IV-C.

TABLE I
ITERATION RESULT OF PCC VOLTAGE IN CASE I

Method	U_{pcc}^{+} (p.u.)	U_{pcc}^{-} (p.u.)
Initial equivalent method with $U_{pcc}^{+}=1$ p.u. and $U_{pcc}^{-}=0$ p.u.	0.253	0.226
Equivalent method 1 with $U_{pcc}^{+}=0.253$ p.u. and $U_{pcc}^{-}=0.226$ p.u.	0.253	0.226
DM	0.253	0.226

Moreover, PMSGs are clustered into three clusters according to the clustering boundaries. The clustering results are shown in Table II. The average active power of PMSGs is displayed in the same figure, as shown in Fig. 12. The characteristics are consistent with the analytical results, which verifies the effectiveness of the clustering method.

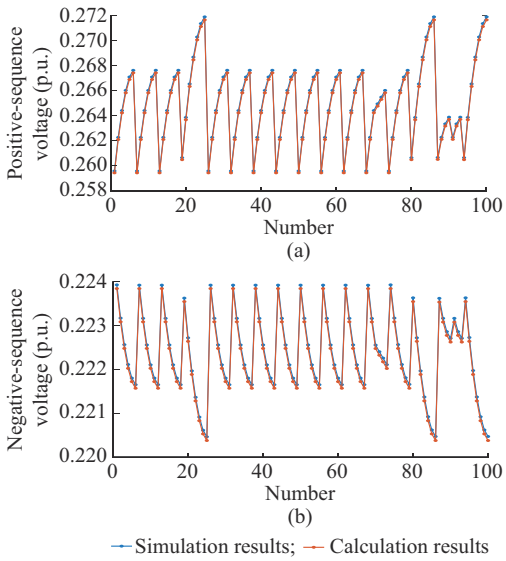

Fig. 11. Terminal voltage of each PMSG. (a) Positive-sequence voltage. (b) Negative-sequence voltage.

TABLE II
CLUSTERING RESULTS

Cluster	Number of PMSGs
I	
II	4-6, 9-12, 16-18, 22-25, 29-31, 36, 37, 41-43, 48, 49, 53-55, 59-61, 64-67, 71-73, 76-79, 82-86, 89, 90, 92, 93, 95-100
III	1-3, 7, 8, 13-15, 19-21, 26-28, 32-35, 38-40, 44-47, 50-52, 56-58, 62, 63, 68-70, 74, 75, 80, 81, 87, 88, 91, 94

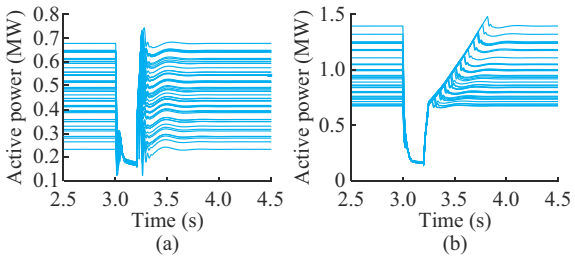

Fig. 12. Average active power of PMSGs in the same cluster in Case I. (a) Cluster II. (b) Cluster III.

The active power, reactive power, and PCC voltages of the DM are compared using the traditional SMEM (SM) in [34], the four-machine equivalent method (FM) in [11], and the three-machine equivalent method (TM), i. e., the proposed dynamic equivalent method. The results are shown in Figs. 13-15. The DM refers to a comprehensive modelling method of the wind farm without any equivalence simplifications, preserving all internal topologies and the structure of each PMSG.

Due to the severe fault, the PMSGs all belong to Clusters II and III. Thus, the active power responses of various equivalent methods are basically the same during the fault. However, the TM represents the recovery characteristic more accurately than SM and FM. The reactive power and the PCC voltage characteristics of various equivalent methods are basically the same.

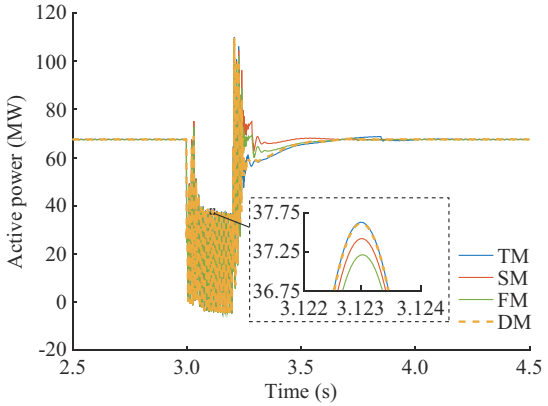

Fig. 13. Active power of various equivalent methods in Case I.

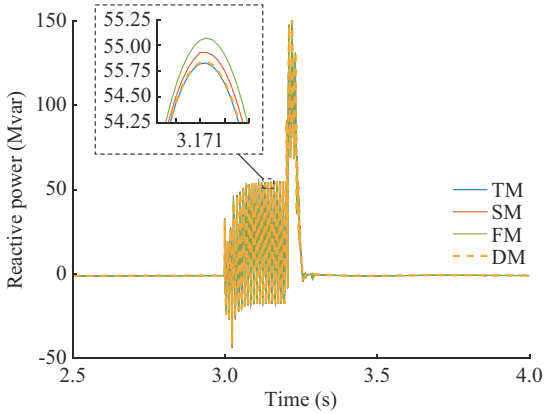

Fig. 14. Reactive power of various equivalent methods in Case I.

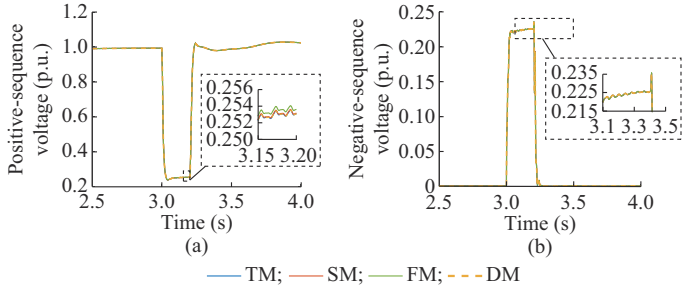

Fig. 15. PCC voltages of various equivalent methods in Case I. (a) Positive-sequence voltage. (b) Negative-sequence voltage.

B. Case II: Single-phase Short-circuit Fault at Bus 30

In Case II, the wind speeds of each PMSG are the same as those in Case I. And a simulation analysis is conducted for a single-phase short-circuit fault with a duration of 0.2 s at bus 30. Compared with Case I, phase A is connected to the ground through a larger resistance of 0.03 Ω and the voltage dip is slighter than that in Case I. Further applying the iterative simulation to solve the PCC voltage, the iteration results are shown in Table III. After two iterations, the positive- and negative-sequence components of the PCC voltage can be obtained. Moreover, according to Section III, the PMSGs can be grouped, and the clustering results are not presented for space reasons. Most of the PMSGs belong to Clusters I and II.

Figure 16 shows the average active power of each PMSG. Figures 17-19 compare the active power, reactive power, and PCC voltages of various equivalent methods.

TABLE III
ITERATION RESULT OF PCC VOLTAGE IN CASE II

Method	U_{pcc}^{+} (p.u.)	U_{pcc}^{-} (p.u.)
Initial equivalent method with $U_{pcc}^{+}=1$ p.u. and $U_{pcc}^{-}=0$ p.u.	0.647	0.361
Equivalent method 1 with $U_{pcc}^{+}=0.647$ p.u. and $U_{pcc}^{-}=0.361$ p.u.	0.646	0.360
DM	0.646	0.360

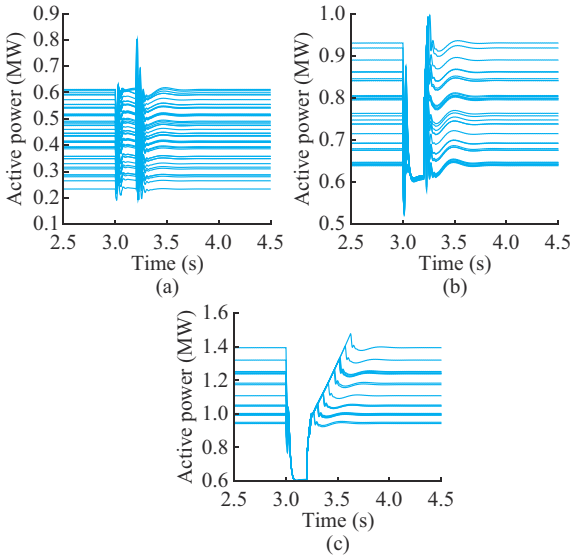

Fig. 16. Average active power of PMSGs in the same cluster in Case II. (a) Cluster I. (b) Cluster II. (c) Cluster III.

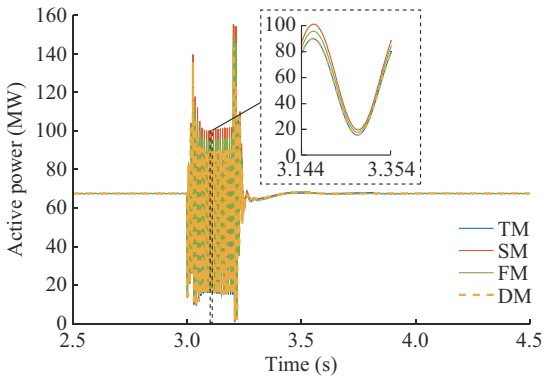

Fig. 17. Active power of various equivalent methods in Case II.

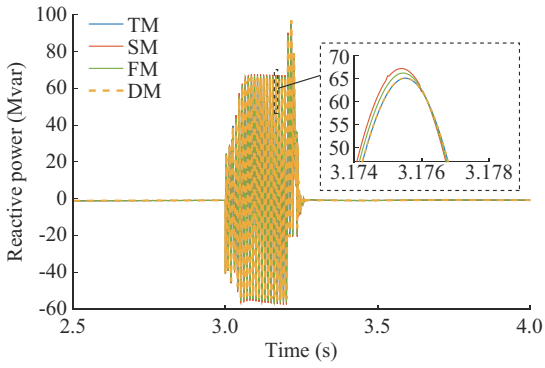

Fig. 18. Reactive power of various equivalent methods in Case II.

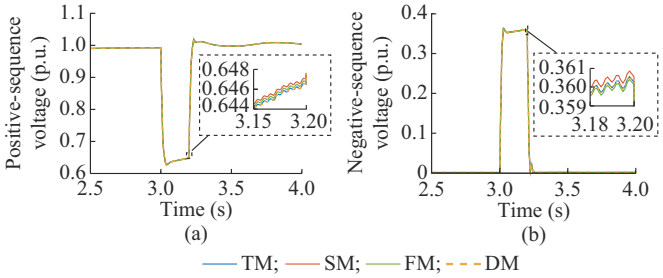

Fig. 19. PCC voltages of various equivalent methods in Case II. (a) Positive-sequence voltage. (b) Negative-sequence voltage.

In Case II, only a small number of PMSGs have a ramp recovery process. Therefore, the SM, FM, and TM are able to perform the active power characteristics accurately after fault clearance. Compared with SM and FM, TM can more accurately present the active power characteristics during the fault, as SM and FM struggle to differentiate accurately between Clusters I and II.

To reflect the effectiveness of the proposed dynamic equivalent method more clearly, we present the average active power of various equivalent methods in Fig. 20. The TM is more accurate after fault clearance in Case I and more accurate during the fault in Case II. In the FM, PMSGs are clustered based on the wind speed. Even though the actual response characteristics of these PMSGs vary under various fault conditions, the clustering results of this method remain unchanged. This renders FM less effective in handling different faults.

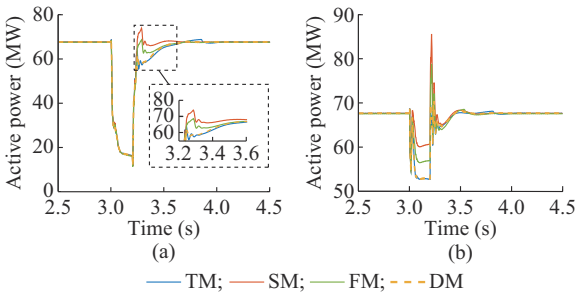

Fig. 20. Average active power of different equivalent methods. (a) Case I. (b) Case II.

In summary, SM and FM cannot reflect the active power differences among PMSGs in different clusters, while the proposed dynamic equivalent method can achieve accurate equivalence under different faults.

C. Case III: Two-phase Short-circuit Fault at Bus 17

To validate the adaptability of the proposed dynamic equivalent method under different wind speeds, fault locations, and fault durations, Case III introduces a two-phase short-circuit fault with a duration of 0.1 s at bus 17. The average wind speed of the wind farm is set to be 9 m/s. Wind speeds for PMSGs are randomly sampled within 9 ± 2 m/s, which are illustrated in Fig. 21.

Similarly, the iterative simulation is used to solve the PCC voltage. The iteration results are presented in Table IV. The PCC voltage also converges to the actual value after two iterations.

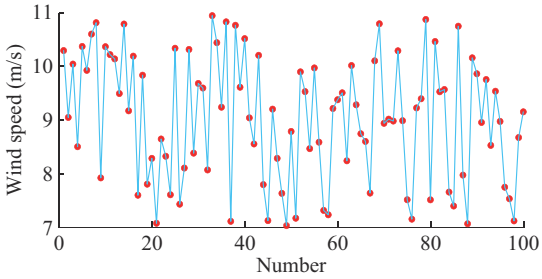

Fig. 21. Wind speeds of PMSGs in Case III.

TABLE IV
ITERATION RESULT OF PCC VOLTAGE IN CASE III

Method	U_{pcc}^{+} (p.u.)	U_{pcc}^{-} (p.u.)
Initial equivalent method with $U_{pcc}^{+}=1$ p.u. and $U_{pcc}^{-}=0$	0.661	0.174
Equivalent method 1 with $U_{pcc}^{+}=0.661$ p.u. and $U_{pcc}^{-}=0.174$	0.661	0.174
DM	0.661	0.174

Moreover, the PMSGs within the wind farm are clustered using the clustering method. The average active power of PMSGs within the same cluster is shown in Fig. 22. It can be observed that the response characteristics of PMSGs in the same cluster are consistent with the theoretical ones.

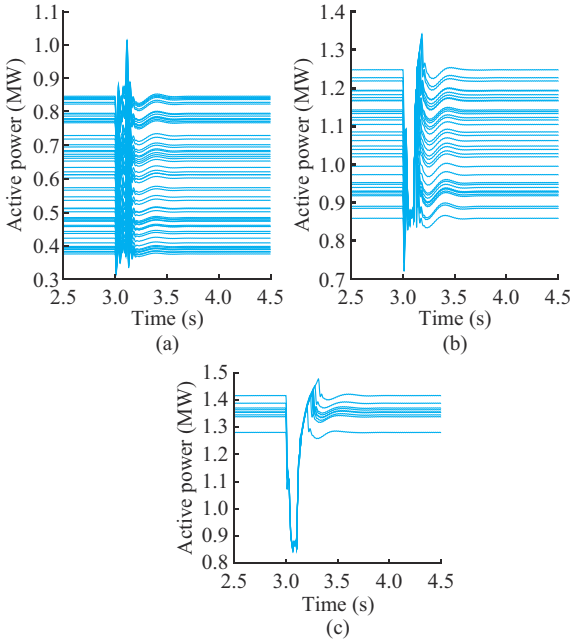

Fig. 22. Average active power of PMSGs in the same cluster in Case III. (a) Cluster I. (b) Cluster II. (c) Cluster III.

Further, the output active power and reactive power of various methods are compared, as shown in Figs. 23-25.

Table V shows the simulation time and the root-mean-square errors (RMSEs) of active power for various methods. The results indicate that the proposed dynamic equivalent method can achieve more accurate equivalence for the wind farm under different wind speeds, fault locations, and fault durations.

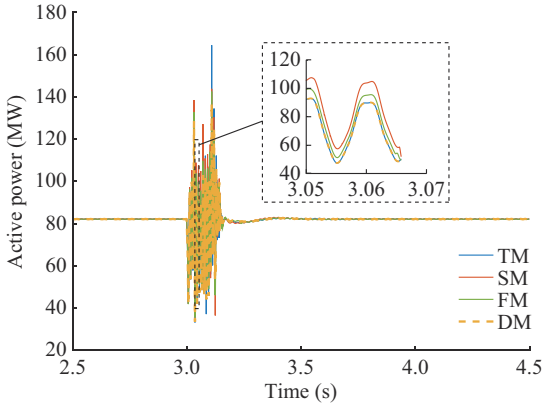

Fig. 23. Active power of various equivalent methods in Case III.

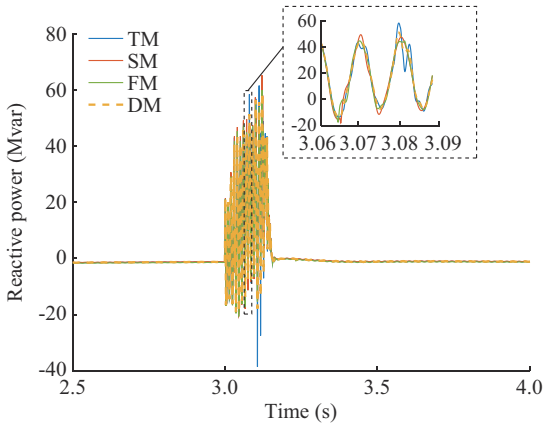

Fig. 24. Reactive power of various equivalent methods in Case III.

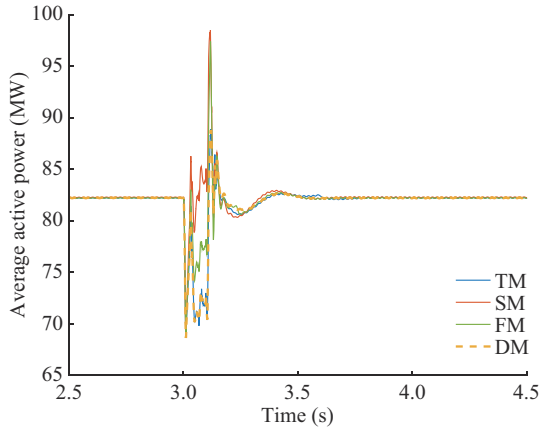

Fig. 25. Average active power of various equivalent methods in Case III.

TABLE V
SIMULATION TIME AND RMSES OF ACTIVE POWER FOR VARIOUS EQUIVALENT METHODS

Method	Case I		Case II		Case III	
	Simulation time (s)	RMSE (%)	Simulation time (s)	RMSE (%)	Simulation time (s)	RMSE (%)
DM	549		491		516	
TM	20	1.23	16	0.41	23	0.39
SM	14	6.10	11	10.01	10	4.51
FM	15	2.90	12	5.84	13	2.27

Moreover, it is also evident that the proposed dynamic equivalent method can significantly improve the simulation efficiency compared with the DM. This is primarily due to the following reasons. ① The terminal voltage calculation process in Section V-A is algebraic calculation, and the time it takes is negligible compared with the simulation time. ② The iterative simulation process in Section V-B is based on the equivalent model. Although it requires multiple iterations, the simulation time per iteration is comparable to that of an SMEM. ③ Before the PCC voltage converges, the simulation process is only carried out until the end-of-fault moment. As a result, while the proposed dynamic equivalent method requires longer simulation time compared with the SM, it still significantly improves simulation efficiency compared with the DM. The simulation time shown in Table V for the proposed dynamic equivalent method represents the sum of the simulation time for multiple iterations, including the time needed for constructing the equivalent model.

VII. CONCLUSION

Under asymmetrical faults, the proposed dynamic equivalent method takes the effects of the fault severity and the negative-sequence control into consideration. The PMSGs are clustered into different clusters according to the characteristics of their active power. Further, equivalent methods are constructed for different clusters of PMSGs, respectively. Moreover, iterative simulation for calculating the clustering indicators is presented and applied to the anticipated faults. Thus, the difficulty in obtaining clustering indicators is solved. Eventually, the proposed dynamic equivalent method is validated on a modified IEEE 39-bus system. The results show that the proposed dynamic equivalent method has good performance in terms of efficiency and accuracy.

It is worth mentioning that the control parameters of each PMSG within the wind farm are set to be consistent for the sake of theoretical study. When the control parameters of each PMSG are different, the proposed dynamic equivalent method is still applicable but needs to be modified appropriately. Taking different reactive current factors K as an example, the proposed dynamic equivalent method requires additional calculations for the clustering boundaries of each PMSG under different K values, as well as the equivalent control parameters of the equivalent model. In addition, the clustering boundaries of each PMSG only need to be computed once and do not require recalculation during application. And the calculation process of equivalent parameters does not cause additional computational load, merely substituting different K values for calculation. Thus, the varying K values of each PMSG have little impact on the efficiency of the proposed dynamic equivalent method.

In the future, the proposed dynamic equivalent method can be applied to DFIGs, PV systems, and wind turbine clusters. When applied to DFIGs, due to the more complex structure and control of DFIGs, their response characteristics are more varied, and it is difficult to analytically solve the clustering boundaries. Therefore, it relies on more complex mechanism analysis when applying the proposed dynamic equivalent method to DFIGs. As for PV systems, their mod-

el structures are fundamentally similar to those of PMSGs. Thus, the proposed dynamic equivalent method can be directly applied to PV systems, with only the need of minor adjustments in the clustering boundaries according to the control methods of PV systems. Regarding wind turbine clusters containing multiple wind farms and other dynamic equipment such as conventional units and constant-impedance loads, these devices also influence the terminal voltage of each wind turbine during faults. Their dynamic characteristics should not be overlooked when applying the solution method of clustering indices in this paper. These aspects can be further studied in the future.

REFERENCES

[1] Y. Wang, Q. Hu, L. Li *et al*., "Approaches to wind power curve modeling: a review and discussion," *Renewable and Sustainable Energy Reviews*, vol. 116, p. 109422, Dec. 2019.

[2] C. E. Council, "2022 national electric reliability annual report," Tech. Rep., National Energy Administration, Oct. 2023.

[3] L. Li, "Study of dynamic equivalent modeling methods of wind farm with DDPMSGs," Ph. D. dissertation, Southwest Jiaotong University, Chengdu, China, 2022.

[4] Y. Jin, P. Ju, C. Rehtanz *et al*., "Equivalent modeling of wind energy conversion considering overall effect of pitch angle controllers in wind farm," *Applied Energy*, vol. 222, pp. 485-496, Jul. 2018.

[5] J. Zou, P. Chao, Y. Yan *et al*., "A survey of dynamic equivalent modeling for wind farm," *Renewable and Sustainable Energy Reviews*, vol. 40, pp. 956-963, Dec. 2014.

[6] P. M. Anderson, *Analysis of Faulted Power Systems*. New York: John Wiley & Sons, 1995.

[7] J. J. Grainger, *Power System Analysis*. New York: McGraw-Hill, 1999.

[8] Ö. Göksu, R. Teodorescu, and P. C. Kjær, "Impact of wind power plant reactive current injection during asymmetrical grid faults," *IET Renewable Power Generation*, vol. 7, no. 5, pp. 484-492, Sept. 2013.

[9] A. Camacho, M. Castilla, J. Miret *et al*., "Flexible voltage support control for three-phase distributed generation inverters under grid fault," *IEEE Transactions on Industrial Electronics*, vol. 60, no. 4, pp. 1429-1441, Jan. 2012.

[10] J. Brochu and C. Larose, "Validation of single- and multiple-machine equivalents for modeling wind power plants," *IEEE Transactions on Energy Conversion*, vol. 26, no. 2, pp. 532-541, Jun. 2011.

[11] W. Li, P. Chao, X. Liang *et al*., "A practical equivalent method for DFIG wind farms," *IEEE Transactions on Sustainable Energy*, vol. 9, no. 2, pp. 610-620, Sept. 2017.

[12] P. Wang, Z. Zhang, Q. Huang *et al*., "Wind farm dynamic equivalent modeling method for power system probabilistic stability assessment," *IEEE Transactions on Industry Applications*, vol. 56, no. 3, pp. 2273-2280, Jan. 2020.

[13] M. Ali, I.-S. Ilie, J. V. Milanovic *et al*., "Wind farm model aggregation using probabilistic clustering," *IEEE Transactions on Power Systems*, vol. 28, no. 1, pp. 309-316, Jul. 2012.

[14] M. Ding and Q. Zhu, "Equivalent modeling of PMSG-based wind power plants considering LVRT capabilities: electromechanical transients in power systems," *SpringerPlus*, vol. 5, no. 1, p. 2037, Nov. 2016.

[15] Y. Gao, Y. Jin, P. Ju *et al*., "Dynamic equivalence of wind farm composed of double fed induction generators considering operation characteristic of crowbar," *Power System Technology*, vol. 39, no. 3, pp. 628-633, Mar. 2015.

[16] J. Zou, C. Peng, H. Xu *et al*., "A fuzzy clustering algorithm-based dynamic equivalent modeling method for wind farm with DFIG," *IEEE Transactions on Energy Conversion*, vol. 30, no. 4, pp. 1329-1337, May 2015.

[17] S. Chen, C. Wang, H. Shen *et al*., "Dynamic equivalence for wind farms based on clustering algorithm," *Proceedings of the CSEE*, vol. 32, no. 4, pp. 11-19, Feb. 2012.

[18] R. Fang, R. Shang, M. Wu *et al*., "Application of gray relational analysis to *k*-means clustering for dynamic equivalent modeling of wind farm," *International Journal of Hydrogen Energy*, vol. 42, no. 31, pp. 20 154-20 163, Aug. 2017.

[19] Y. Xue, Z. Zhang, and Z. Xu, "A dynamic equivalent aggregation method of wind turbine systems with a full-scale power converter for electromagnetic transient simulations," *IET Renewable Power Generation*, vol. 17, no. 1, pp. 36-51, Jan. 2023.

[20] Z. Wang, G. Yang, Y. Tang *et al*., "Modeling method of direct-driven wind generators wind farm based on feature influence factors and improved BP algorithm," *Proceedings of the CSEE*, vol. 39, no. 9, pp. 2104-2615, May 2019.

[21] D. Li, C. Shen, Y. Liu *et al*., "A dynamic equivalent method for PMSG-WTG based wind farms considering wind speeds and fault severities," *IEEE Transactions on Power Systems*, vol. 39, no. 2, pp. 3738-3751, Mar. 2024.

[22] S. Alepuz, S. Busquets-Monge, C. A. Silva *et al*., "Control strategies based on symmetrical components for grid-connected converters under voltage dips," *IEEE Transactions on Industrial Electronics*, vol. 56, no. 6, pp. 2162-2173, Mar. 2009.

[23] Y. Hu, Z. Zhu, and M. Odavic, "Instantaneous power control for suppressing the second-harmonic DC-bus voltage under generic unbalanced operating conditions," *IEEE Transactions on Power Electronics*, vol. 32, no. 5, pp. 3998-4006, Jun. 2016.

[24] T. Neumann, T. Wijnhoven, and I. Erlich, "Enhanced dynamic voltage control of type 4 wind turbines during unbalanced grid faults," *IEEE Transactions on Energy Conversion*, vol. 30, no. 4, pp. 1650-1659, Sept. 2015.

[25] *Technical Specification for Connecting Wind Farm to Power System – Part 1: Onshore Wind Power*, GB/T19963.1-2021, 2021.

[26] C. Feltes, S. Engelhardt, J. Kretschmann *et al*., "Comparison of the grid support capability of DFIG-based wind farms and conventional power plants with synchronous generators," in *Proceedings of 2009 IEEE PES General Meeting*, Calgary, Canada, Jul. 2009, pp. 1-7.

[27] J. Fortmann, S. Engelhardt, C. Feltes *et al*., "New generic model of dfg-based wind turbines for RMS-type simulation," *IEEE Transactions on Energy Conversion*, vol. 29, no. 1, pp. 110-118, Nov. 2013.

[28] Z. Guo and W. Wu, "Data-driven model predictive control method for wind farms to provide frequency support," *IEEE Transactions on Energy Conversion*, vol. 37, no. 2, pp. 1304-1313, Nov. 2021.

[29] T. Wang, S. Huang, M. Gao *et al*., "Adaptive extended Kalman filter based dynamic equivalent method of PMSG wind farm cluster," *IEEE Transactions on Industry Applications*, vol. 57, no. 3, pp. 2908-2917, Jan. 2021.

[30] W. Li, P. Chao, X. Liang *et al*., "An improved single-machine equivalent method of wind power plants by calibrating power recovery behaviors," *IEEE Transactions on Power Systems*, vol. 33, no. 4, pp. 4371-4381, Nov. 2017.

[31] M. Garcia-Gracia, M. P. Comech, J. Sallan *et al*., "Modelling wind farms for grid disturbance studies," *Renewable Energy*, vol. 33, no. 9, pp. 2109-2121, Sept. 2008.

[32] Y. Song, Y. Chen, Z. Yu *et al*., "CloudPSS: a high-performance power system simulator based on cloud computing," *Energy Reports*, vol. 6, pp. 1611-1618, Dec. 2020.

[33] CloudPSS. (2016, Dec.). CloudPSS platform. [Online]. Available: https://www.cloudpss.net/

[34] M. Mercado-Vargas, D. Gómez-Lorente, and E. Alameda-Hernandez, "Aggregated models of permanent magnet synchronous generators wind farms," *Renewable Energy*, vol. 83, pp. 1287-1298, Nov. 2015.

Dongsheng Li received the B.E. degree in electrical engineering from Wuhan University, Wuhan, China, in 2019, and the Ph.D. degree in electrical engineering from Tsinghua University, Beijing, China, in 2024. His research interest includes equivalent modeling of wind turbines.

Zetian Zheng received the B.E. and Ph.D. degrees in electrical engineering from Tsinghua University, Beijing, China, in 2017 and 2023, respectively. His research interests include power system stability and control.

Chen Shen received the B.E. and Ph.D. degrees in electrical engineering from Tsinghua University, Beijing, China, in 1993 and 1998, respectively. From 1998 to 2001, he was a Postdoc Research Fellow with the Department of Electrical Engineering and Computer Science, University of Missouri Rolla, Rolla, USA. Since 2009, he has been a Professor with the Department of Electrical Engineering, Tsinghua University. He is currently the Director of the Energy Digitization Research Center, Sichuan Energy Internet Research Institute, Tsinghua University, Chengdu, China. His research interests include power system analysis and control, renewable energy generation, and smart grid.